Asia-Pacific Journal of Atmospheric Sciences (2024) 60:669–678
https://doi.org/10.1007/s13143-024-00373-5

Online ISSN 1976-7951
Print ISSN 1976-7633

ORIGINAL ARTICLE

Zonal Contrasts of the Tropical Pacific Climate Predicted by a Global Constraint

Sukyoung Lee[1] · Peter R. Bannon[1] · Mingyu Park[2] · Joseph P. Clark[2]

Received: 19 March 2024 / Revised: 29 May 2024 / Accepted: 10 June 2024 / Published online: 12 July 2024

Abstract

The zonal gradients in sea surface temperature and convective heating across the tropical Pacific play a pivotal role in setting the weather and climate patterns globally. Under global warming, the current generation of climate models predict that the zonal gradients will decrease, but the trajectory of the observed trends is the opposite. Theories supporting either of the two projections exist, but there are many relevant processes whose net effect is unclear. In this study, a global constraint – the maximum material entropy production (maxMEP) hypothesis—is considered to help close the gap. The climate system considered here is comprised of a one-layer atmosphere and surface in six regions that represent the western tropical Pacific, eastern tropical Pacific, northern and southern midlatitudes, and northern and southern polar regions. The model conserves energy but does not explicitly include dynamics. The model input is observation-based radiative parameters. The radiative effect of greenhouse gas (GHG) loading is mimicked by prescribing increases in the longwave absorptivity ϵ. The model solutions predict that zonal contrasts in surface temperature, convective heat flux, and surface pressure increase with increasing ϵ. While maxMEP solutions in general cannot provide a definite answer to the problem, these model results strengthen the possibility that the trajectory of the observed trend reflects the response to increasing GHG loading in the atmosphere.

Keywords Tropical Pacific climate · Zonal contrasts · Entropy · Global constraint

1 Introduction

The zonal gradients of the sea surface temperature (SST) and convective heating in the tropical Pacific have profound impacts on weather and climate globally. Therefore, the accuracy of the future climate projections around the globe critically depends on the trends in these zonal gradients. Climate model simulations generally show decreasing zonal SST gradients over the past century, but recent analyses of the observational records show increasing zonal SST gradients (Seager et al. 2019, 2022; Lee et al. 2022). Midlatitude responses to the tropical Pacific SST gradients are realized through its impact on local convective heating that then generates poleward propagating Rossby wave trains (Hoskins and Karoly 1981). Since at least 1979, the zonal gradient of the convective heating has also been strengthening (Park and Lee 2022). Resolving these diverging projections is challenging because the models are never perfect, and the observational trajectories are subject to internal variability in addition to the greenhouse gas forcing.

As was recently reviewed (Lee et al. 2022), some theories advocate the model simulations of an El Niño-like future while others favor the observed La-Nina trajectories. The key component of these theories ranges from tropical dry static stability (Knutson and Manabe 1995), uneven evaporative cooling caused by uneven SST (Knutson and Manabe 1995; Xie et al. 2010), gross moist stability (Chou et al. 2013; Wills et al. 2017) and equatorial Pacific ocean circulation (Clement et al. 1996). More recently, the cooling of the Southern Ocean (SO) surface water has been pointed out as being a contributor to the observed La Niña-like trend (Dong et al. 2022), possibly aided by the Antarctic ozone hole (Hartmann 2022), rather than by the greenhouse gas forcing. Each one of these ideas stems from considerations of a subset of physical processes that occur in nature and in models. While ideas of these specific physical processes are helpful toward resolving the issue, it is often challenging to

✉ Sukyoung Lee
sxl31@psu.edu

[1] Department of Meteorology and Atmospheric Science, The Pennsylvania State University , University Park, PA 16802, USA

[2] Program in Atmospheric and Oceanic Sciences, Princeton University, Princeton, NJ, USA

test the hypothesized mechanisms and to determine which processes are significant. Moreover, given the large degrees of freedom in the climate system, it is likely that there are many other physical processes not yet even considered but are relevant to the problem. In this regard, predictions based on some sort of global constraint could play a useful role.

The maximum material entropy production (MEP) hypothesis offers such a global constraint. Paltridge (1975) was the first one who showed that if a simple climate system is constrained to achieve a maxMEP state, the resulting solutions of latitudinal distributions of zonal mean temperature, fractional cloud cover, and meridional heat flux closely resemble the observations. In their review of the subject, Ozawa et al. (2003) showed that a maxMEP state corresponds to a state where the rate of entropy production caused by turbulent dissipation is maximized. They also showed that the maxMEP hypothesis is equivalent to Lorenz's conjecture (Lorenz 1960) that given solar radiation, the latitudinal temperature distribution corresponds to the state of maximum possible rate of generation of available potential energy.

As was more recently reviewed by Singh and O'Neill (2022), however, the maxMEP hypothesis is controversial, one reason being that it is not derived from the governing equations of the climate system; hence it has no clear physical basis. One of the studies cited in that review relevant for climate is Goody (2007) who examined the maxMEP solution of the two-box (tropical and extratropical) climate system for Earth, Venus, Mars, and Titan. He found that the solutions do not agree with the observations *quantitatively*, hence concluded that the maxMEP, constrained only by energy and mass conservation, cannot calculate the state of these planets' climate. However, he acknowledged that the maxMEP is useful for *qualitative* estimates of climate states or as an aid to choose between independent climate projections.

In fact, Goody's conclusion that maxMEP has a place in projecting future climate is in line with the suggestion by Dewar (2009) which is based on the idea of Jaynes (1957). Jaynes (1957) showed that maximizing Shannon's information entropy (Shannon 1948) subject to certain partial knowledge yields a result which can completely describe thermodynamic properties of a system except for the presence of Boltzmann's constant. From this result, Jaynes (1957) concluded that statistical mechanics can be thought of as a form of statistical inference. If maxMEP is equivalent to Jaynes' maximum entropy principle (Dewar 2003, 2005), which although is yet to be demonstrated (Bruers 2007; Dewar 2009; Grinstein and Linsker 2007), we may view our solutions subjected to maxMEP as statistical inferences based on partial knowledge (energy conservation in our problem); paraphrasing Jaynes (1957), the solutions represent the best estimates given the information provided in the system under consideration. The details of our model system and information that we provide to our model will be described in Sect. 2, and the implications and limitations of our solutions will be discussed in Sect. 4.

With this general outlook, our specific goal is to estimate how zonal contrasts in SST and convective heating would change as greenhouse gas (GHG) loading increases. Our approach is to compare surface temperature, surface pressure, and convective heat flux solutions of our control run with those of 'GHG' runs where long-wave absorptivity values in the atmospheric boxes are uniformly raised from their control values. As such, in this study the maxMEP approach is used to determine the sensitivity of the solution to the long-wave absorptivity values, rather than predicting the mean state of a climate system. The latter was carried out relatively recently by Pascale et al. (2012) who found that under realistic insolation, their maxMEP solution captures the observed meridional temperature distribution and heat flux with reasonable accuracy. Our model setup resembles theirs, with the major difference being the division of the tropics into two regions in our model which allows for the investigation of zonal gradient sensitivity to the longwave absorptivity.

2 The Model

2.1 Model Configuration

The model system consists of multiple, horizontally homogenous regions comprised of two isothermal layers (e.g., Hartmann 2016; Sect. 3.8): one atmospheric layer overlaying a surface layer. The atmospheric layer represents the entire column of the atmosphere. The layer designation index k is used for the surface ($k = 1$) and the atmosphere ($k = 2$). Horizontally the Pacific sector of the globe is divided into western and eastern tropical Pacific regions, midlatitude and polar Northern Hemisphere (NH) regions, and midlatitude and polar Southern Hemisphere (SH) regions. Figure 1 provides a schematic description of the model. The region designation index r is used for western tropical Pacific ($r = 1$), eastern tropical Pacific ($r = 2$), NH midlatitudes ($r = 3$), SH midlatitudes ($r = 4$), NH polar ($r = 5$), and SH high polar ($r = 6$) regions. Three model configurations are considered in our analyses: The first configuration is comprised of only the two tropical regions, $r = \{1, 2\}$ (henceforth the Two-Region model); the second configuration includes the two tropical regions plus the two midlatitude regions, $r = \{1, 2, 3, 4\}$ (the Four-Region model); the third configuration includes all six regions, $r = \{1, 2, 3, 4, 5, 6\}$ (the Six-Region model). The goal of examining these three configurations is to evaluate the sensitivity of the zonal gradients in the tropical Pacific to the inclusion of the extratropics. A

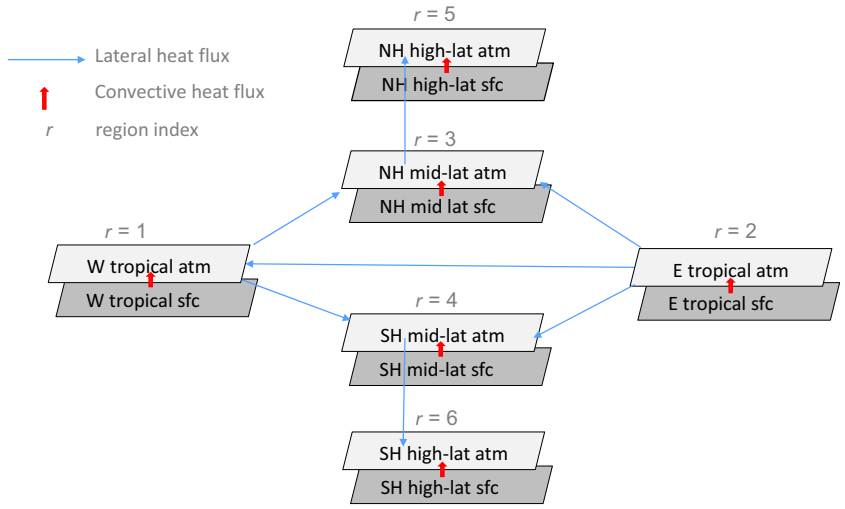

Fig. 1 A schematic of the Six-Region model. If the two high latitude regions are removed, this model reduces to the Four-Region model; if the two mid latitude regions are also removed, the model reduces to the Two-Region model. The red vertical arrows denote convective heat flux from the surface to the atmosphere, and the blue arrows represent lateral heat flux between adjacent regions. In this diagram, the direction of the blue arrows is chosen to resemble the lateral heat fluxes in the current climate; depending on the input radiative parameters the directions may reverse

schematic representation of the Six-Region setup is shown in Fig. 1. In the Four-Region model, the high latitude regions are absent; in the Two-Region model, only the two tropical regions are present.

The prescribed variables are the area (A) of each region, the absorbed shortwave radiation (ASR) at the top-of-atmosphere (TOA) and at the surface, atmospheric shortwave absorptivity (a_{sw}), and atmospheric longwave absorptivity (ϵ). The value of a_{sw} is computed as: $a_{sw} = [ASR(TOA) - ASR(sfc)]/ASR(TOA)$, where ASR(sfc) is downward minus upward shortwave radiative flux at surface. These input values are derived from the ERA5 product for 1979–2020. The input radiative flux values for the models are listed in Table 1 along with the area of each of the box domains and surface temperatures. These shortwave radiation input parameters are fixed at the same value for all calculations presented here. Therefore, effects of GHG forcing on albedo and shortwave absorptivity are not considered. Although observation-based radiative flux is used to prescribe the input values for our model, as was stated earlier, the solutions that we seek from this model – temperature of each box and energy flux between neighboring boxes—are not meant to be quantitatively compared with observations. Instead, the goal is to provide qualitative descriptions of how this idealized climate system responds to increased long-wave absorptivity which mimics greenhouse gas forcing.

At each region r, the heating in the kth layer caused by the shortwave, $\dot{q}_{sw}(k)$, equals the product of the shortwave absorption coefficient and the downward solar radiation in that layer:

Table 1 Area-averaged values of ASRs, atmospheric shortwave absorptivity a_{sw}, and surface temperature for the indicated domains derived from ERA5 reanalysis for the period of 1979–2020. The values of the atmospheric longwave absorptivity a_{lw} are calculated from our model that best describes the surface temperature differences between the regions. More details are provided in the main text

Regions (r)	ASR(TOA) (Wm^{-2})	ASR(sfc) (Wm^{-2})	a_{sw}	ϵ	Area (10^7 km^2)	Surface Temp (K)
West Pacific ($r=1$) (120°E-180, 30°S-30°N)	303.90	207.63	0.317	0.95	4.25	300.46
East Pacific ($r=2$) (180-70°W, 30°S-30°N)	308.91	216.39	0.301	0.84	7.79	298.36
NH midlatitudes ($r=3$) (30°N-60°N)	216.36	142.02	0.349	0.82	9.33	283.71
SH midlatitudes ($r=4$) (30°S-60°S)	211.17	142.37	0.330	0.93	9.33	284.53
NH high latitudes ($r=5$) (60°N-90°N)	109.40	59.26	0.48	0.95	3.42	265.12
SH high latitudes ($r=6$) (60°S-90°S)	92.92	52.09	0.46	0.95	3.42	256.02

$$\dot{q}_{sw}(k) = a_{sw}(k)sw\downarrow(k)$$

where $a_{sw}(k)$ is shortwave absorptivity and $sw\downarrow(2)$ is a prescribed absorbed solar radiation (ASR) at the top of atmosphere (TOA). The heating by longwave absorption and emission at surface is

$$\dot{q}_{lw}(1) = \epsilon(2)\sigma T^4(2) - \epsilon(1)\sigma T^4(1)$$

and in the atmosphere

$$\dot{q}_{lw}(2) = \epsilon(1)\sigma T^4(1) - 2\epsilon(2)\sigma T^4(2)$$

The TOA outgoing longwave radiation (OLR) is

$$OLR = -(1-\epsilon(2))\epsilon(1)\sigma T^4(1) - \epsilon(2)\sigma T^4(2)$$

Because the surface is assumed to be a blackbody, $\epsilon(1) = 1$. For readability, surface temperature $T(1)$ is denoted as T_{sfc} in Sect. 3 and onward.

Energy conservation requires

$$\sum_{r=1}^{NR} ar(r)ASR(r) + \sum_{r=1}^{NR} ar(r)OLR(r) = 0,$$

where NR is the number of regions and $ar(r)$ is the fractional surface area of the regions whose sum is required to be unity.

In a steady state, the energy budget for the kth layer in a column is given by a balance in the sum of the heatings.

$$\dot{q}_{sw}(k) + \dot{q}_{lw}(k) + \dot{q}_{mat}(k) = 0$$

Where the term $\dot{q}_{mat}(k)$ is the material heating in layer k due to the convergence of the material fluxes of heat. The surface and atmosphere are coupled by a convective heat flux, $chf(k)$. Additionally, the layers are coupled horizontally by a regional lateral heat fluxes between region r and $r\prime$. They are denoted as $rlhf(2, r, r\prime)$. Surface lateral fluxes are set zero. The lateral flux may be positive, toward the region r and away from the region $r\prime$, $rlhf > 0$, or negative, away from the region, $rlhf < 0$. The total material heating is

$$\dot{q}_{mat}(k) = \dot{q}_{chf}(k) + \dot{q}_{lhf}(k) \tag{1}$$

where the convective heating for the surface is $\dot{q_{chf}}(1) = -chf(1)$ and for the atmosphere $\dot{q_{chf}}(2) = chf(1)$. The lateral heating for the atmosphere ($k = 2$) is $\dot{q}_{lhf}(k) = lhf(k, r) = \sum_{r\prime=1}^{NR} rlhf(k, r, r\prime)alhf(r, r\prime)$. Here $alhf$ is the relative area matrix with $alhf(r, r\prime) = \frac{ar(r)}{ar(r\prime)}$ and $alhf(r\prime, r\prime) = 0$. The lateral surface fluxes are zero: $\dot{q_{lhf}}(k = 1) = 0$.

The temperatures and the heating produced by the convective and lateral fluxes, chf and $rlhf$ in each layer, are determined by the constraint that the material entropy production (MEP) of the total system is a maximum: Taking the Two-Region model as an example, there are four equations, each describing energy balance for the four boxes, but there are seven unknown variables which are the four temperatures and three fluxes (see Fig. 1). The maxMEP constraint allows one to determine the seven unknown variables with only four equations.

For this model, the total production is.

$$\dot{\Sigma}_{mat} = \sum_{k=1}^{2} \dot{\sigma}_{mat}(k)$$

Where the production at the kth layer is $\dot{\sigma}_{mat}(k) = \dot{q}_{mat}(k)/T(k)$. The maximization process uses the Nelder and Mead (1965) algorithm (MATLAB function fminsearch) to find the values of the convective and lateral fluxes that produce the maximum MEP. The values of $\dot{q}_{mat}(k)$ are determined from the definition (1). Because this definition generally contains three flux terms at each layer (i.e., one convective flux and two lateral fluxes), their values found by the algorithm are, in general, not unique but the values of the total material heating (1) are. The uniqueness of the total heating (1) assures that the results for the temperatures are unique.

In the steady state, the entropy production processes balance, and their sum vanishes. Mathematically we have, for the kth layer in a column,

$$\dot{\sigma}_{sw}(k) + \dot{\sigma}_{lw}(k) + \dot{\sigma}_{mat}(k) = 0$$

Where the generic rate of entropy production is.

$$\dot{\sigma}(k) = \frac{\dot{q}(k)}{T(k)}$$

2.2 Radiative Input Parameters

The radiative physics is that of a semi-grey atmosphere in local thermodynamic equilibrium above black surfaces. The net effect of shortwave scattering is included with the assumption of a prescribed absorbed solar radiation $\mathrm{ASR}(r) = (1 - \alpha_p(r))\ \mathrm{ISR}(r)$ where $\alpha_p(r)$ is the planetary albedo and ISR is the prescribed incoming solar radiation. As stated earlier, the shortwave and absorptivity used in the base state model are summarized in Table 1.

Unlike solar radiation, longwave radiation is emitted by both the atmosphere and the surface, making the calculation

Table 2 Base-state atmospheric longwave absorptivity ϵ_0 for the six regions for the four specified $\epsilon_0(1)$ given by the left-hand column

Region 1	Region2	Region 3	Region 4	Region 5	Region 6
0.8000	0.6759	0.6271	0.7378	0.6856	0.6665
0.8500	0.7308	0.6947	0.8002	0.7770	0.7643
0.9000	0.7860	0.7613	0.8633	0.8644	0.8591
0.9500	0.8412	0.8283	0.9257	0.9522	0.9530

of the atmospheric longwave absorptivity for each region challenging. In previous studies of maxMEP, ϵ was set at some reasonable values based on observations. This is a viable option here as well, but because the goal of our study is to find out how temperature difference between the two tropical regions changes as the longwave absorptivity increases, it is desirable to start with a base state in which the temperature difference resembles the observed mean state. Therefore, we tune the base values of ϵ, ϵ_0, such that the model temperature difference matches the observed temperature difference. Here the subscript 0 refers to the base state.

For the tuning, we adopted the following procedure. We set the absorptivity of the Western Pacific $\epsilon_0(\mathrm{r}=1)=0.9500$. Then we do a 'double' search for the absorptivity of the Eastern Pacific $\epsilon_0(\mathrm{r}=2)$ that produces the smallest rms skin temperature difference to that observed while also maximizing the entropy production of the entire system. We find $\epsilon_0(\mathrm{r}=2)=0.8412$. With the Pacific absorptivities determined, an analogous double search is then used to find the midlatitude absorptivities of $\epsilon_0(\mathrm{r}=3,\ 4)=0.8282$ and 0.9257. Lastly, with the absorptivities determined for the non-polar regions, the polar regions are then determined by minimizing the rms skin temperature difference and maximizing the total MEP. We find $\epsilon_0(\mathrm{r}=5,\ 6)=0.9522$ and 0.9530. This procedure yields the entries in Table 2 for $\epsilon_0(\mathrm{r}=1)=0.9500$. The sensitivity of the solutions to the choice of $\epsilon_0(r=1)$ value is examined by also considering the additional values of 0.9000, 0.8500, and 0.8000. The absorptivity values for all the cases are listed in Table 2.

3 Results

We now seek a qualitative assessment of how the tropical Pacific zonal gradients in temperature and surface heat flux would change as the longwave absorptivities of the control runs in Table 2 are increased incrementally by an amount $\Delta\epsilon$. In these 'GHG' runs, the value of $\Delta\epsilon$ is increased uniformly across all regions by increments of 0.01. Specifically, using the radiative input parameters including $\epsilon_0+\Delta\epsilon$, we obtain temperatures and material fluxes using the maxMEP constraint.

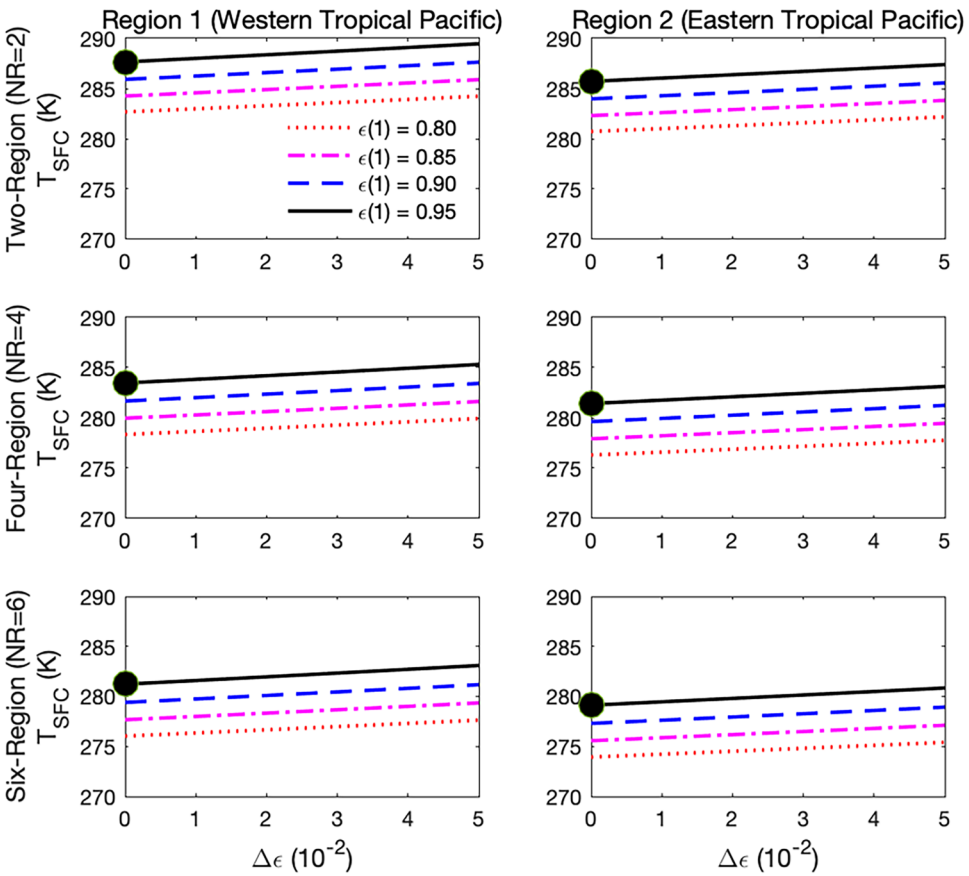

Fig. 2 Sensitivity of T_{sfc} to increasing GHG forcing $\Delta\epsilon$. The left column is for the western tropical Pacific region ($r=1$) and the right column is for the eastern tropical Pacific region ($r=2$). The top row is from the Two-Region model, the middle row from the Four-Region model, and the bottom row from the Six-Region model. The filled circles indicate the solution to the control run. In the subsequent plots, the filled circles are not included

3.1 Sensitivity of Surface Temperature and Convective Heat Flux to GHG Forcing $\Delta\epsilon$

The greenhouse effect tells us that surface temperature T_{sfc} must increase as the atmospheric longwave greenhouse forcing ϵ increases. Figure 2 confirms this expectation. In this figure, the control runs are indicated with the filled circles. To this end, we recall that r is the region index with 1 being western tropical Pacific. In each of the six panels, a comparison amongst the four lines shows that T_{sfc} increases with ϵ_0. Given the base values, we also see that T_{sfc} increases monotonically with $\Delta\epsilon$. Figure 2 also shows the sensitivity to the inclusion of extratropical regions. We see that tropical T_{sfc} in Four-Region model is systematically lower than that of the Two-Region model, and tropical T_{sfc} in Six-Region model are still lower than that of the Four-Region model. This behavior is to be expected because the tropical regions are cooled by poleward heat transport into the midlatitudes in the Four-Region model, and additionally to the high latitudes in the Six-Region model.

In the Earth's climate system, heating of the surface by radiation is balanced by cooling through surface turbulent fluxes (e.g., Trenberth et al. 2009). Therefore, convective heat flux (*chf*) from surface to the atmosphere is expected to increase with increasing values of ϵ_0 and $\Delta\epsilon$. The solutions presented in Fig. 3 indeed show this anticipated behavior. Once again, the convective heat flux in the two tropical regions decreases as the extratropical regions are added to the system.

3.2 Sensitivity of Zonal Gradients in Tropical Pacific Climate to GHG Forcing $\Delta\epsilon$

Having confirmed that T_{sfc} and *chf* depend on ϵ_0 and $\Delta\epsilon$ as expected from the physical grounds, we next examine the sensitivity of zonal gradient between the two tropical boxes to $\Delta\epsilon$, the main result of this study. The results are shown in Fig. 4. The ordinates in Fig. 4 are eastern-minus-western region (Δ_x) values, with the values becoming more negative upward except for $\Delta_x ln\, P_{sfc}$. This convention is adopted because the more negative the values, the greater the zonal contrast. The first row of Fig. 4 shows that $\Delta_x T_{sfc}$ increases with $\Delta\epsilon$, indicating that as GHG loading is increased (greater $\Delta\epsilon$), the western region warms faster than the eastern region. By construction (see Sect. 2), $\Delta_x T_{sfc}$ is made to be independent of Region 1's base value, $\epsilon_0(r = 1)$, which ranges from 0.80 to 0.95 and this is confirmed in Fig. 4.

In this model, the Walker circulation strength can be measured by zonal gradient of surface pressure. We obtained the surface pressure assuming the hydrostatic balance. A single-layer atmosphere such as the one in our model is isothermal. Therefore, integrating the hydrostatic equation, we

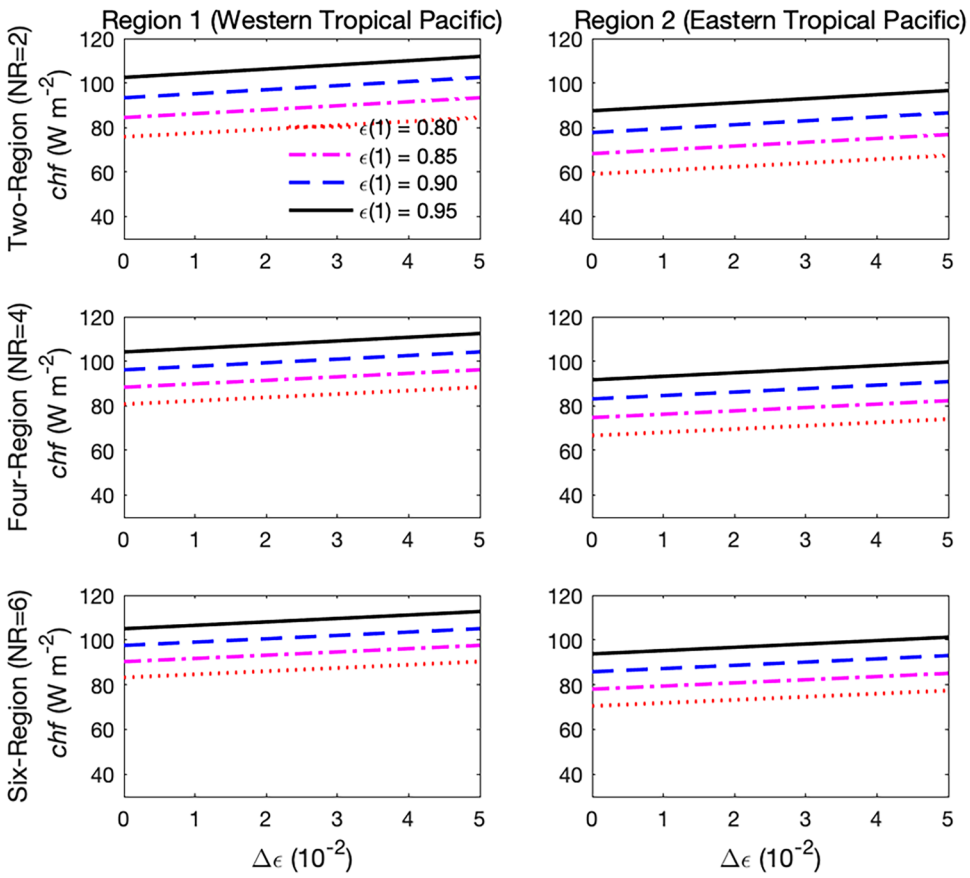

Fig. 3 Sensitivity of *chf* to increasing GHG forcing $\Delta\epsilon$. The left column is for the western tropical Pacific region ($r = 1$) and the right column is for the eastern tropical Pacific region ($r = 2$). The top row is from the Two-Region model, the middle row from the Four-Region model, and the bottom row from the Six-Region model

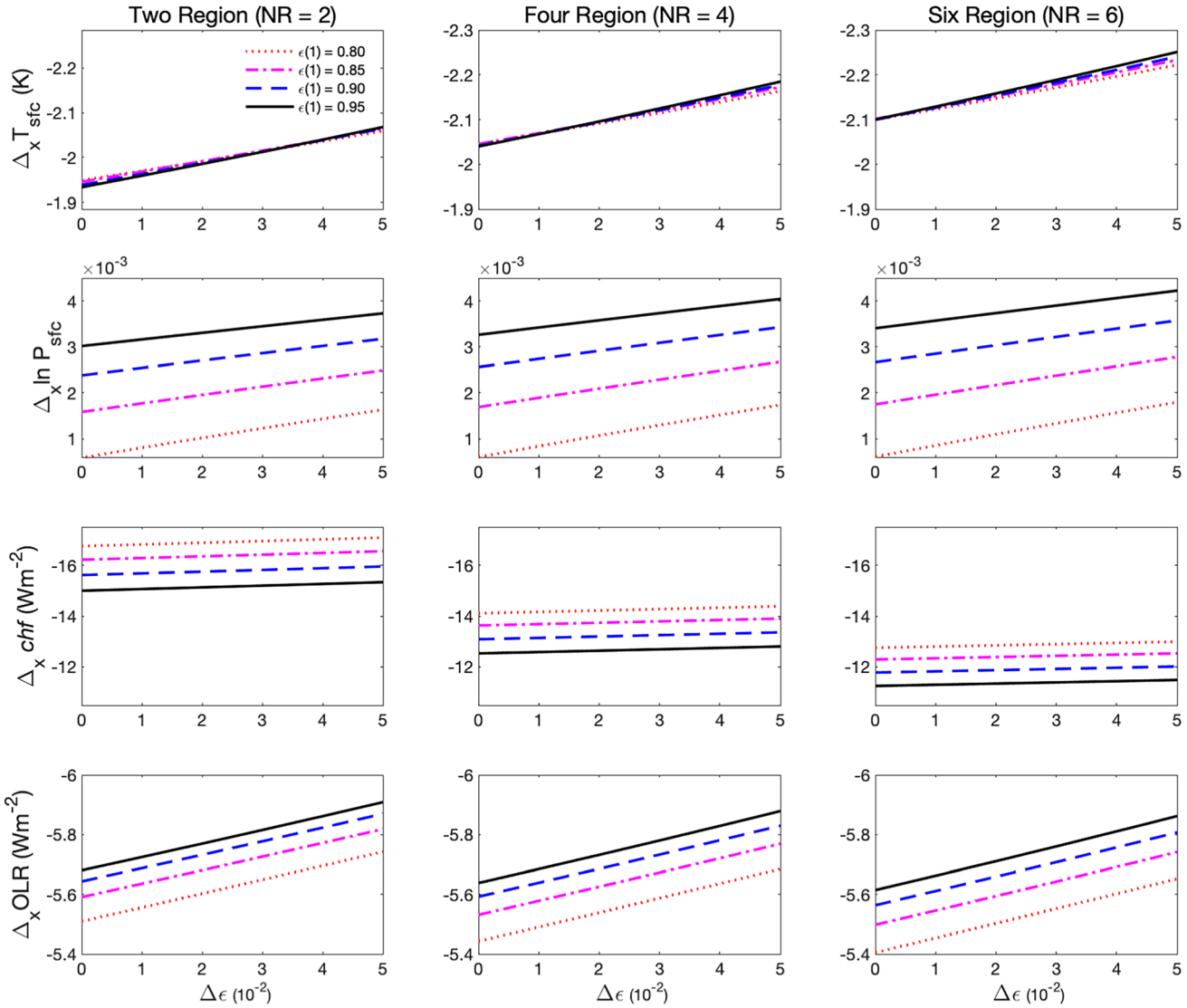

Fig. 4 Sensitivity of zonal gradients in T_{sfc} (first row), $\ln P_{sfc}$ (second row), *chf* (third row), and OLR (forth row) to ϵ and $\Delta\epsilon$. The first column is from the Two-Region model, the second from the Four-Region model, and the third from the Six-Region model

have $lnp(z_{top}) - lnp(z_{sfc}) = -\frac{g}{RT_a}(z_{top} - z_{sfc})$, where z_{top} is the height of the top of the atmosphere, z_{sfc} is the surface height, and T_a is the atmospheric temperature. Assuming that $p(z_{top})$ does not vary in x and by setting $z_{sfc} = 0$, the zonal gradient of surface pressure $p(z_{sfc})$ can be written as $\Delta_x lnp(z_{sfc}) = \frac{gz_{top}}{R}\left[\frac{1}{T_a(E)} - \frac{1}{T_a(W)}\right]$, where E and W within the parentheses refers to the eastern and western region, respectively. In Fig. 4, the values of $\Delta_x lnp_{sfc}$ are obtained with $z_{top} = 10$ km, where $p_{sfc} = p(z_{sfc})$.

The second row of Fig. 4 shows that the surface pressure (P_{sfc}) difference between the eastern and western regions increases with$\Delta\epsilon$, indicating that the maxMEP solution predicts a strengthening Walker circulation as GHG loading increases. Convective heating's zonal contrast also increases with$\Delta\epsilon$, indicating the western region's *chf* increases more rapidly than the eastern region's *chf* does. These temperature, pressure, and convective heating dependencies on $\Delta\epsilon$ can be seen for all four base ϵ cases and for all model configurations.

The model solution indicates the OLR sensitivity to $\Delta\epsilon$ is greater in the western than in the eastern region. As a result, the zonal contrast in OLR increases with $\Delta\epsilon$ (fourth row in Fig. 4). The lower OLR in the western region, compared with the eastern region, stems from the difference between the surface and atmospheric temperatures being greater there. Even though our model does not include clouds, it is interesting that the maxMEP solution predicts a lower OLR in the western region than the eastern region by predicting a lower atmospheric temperature relative to the surface temperature.

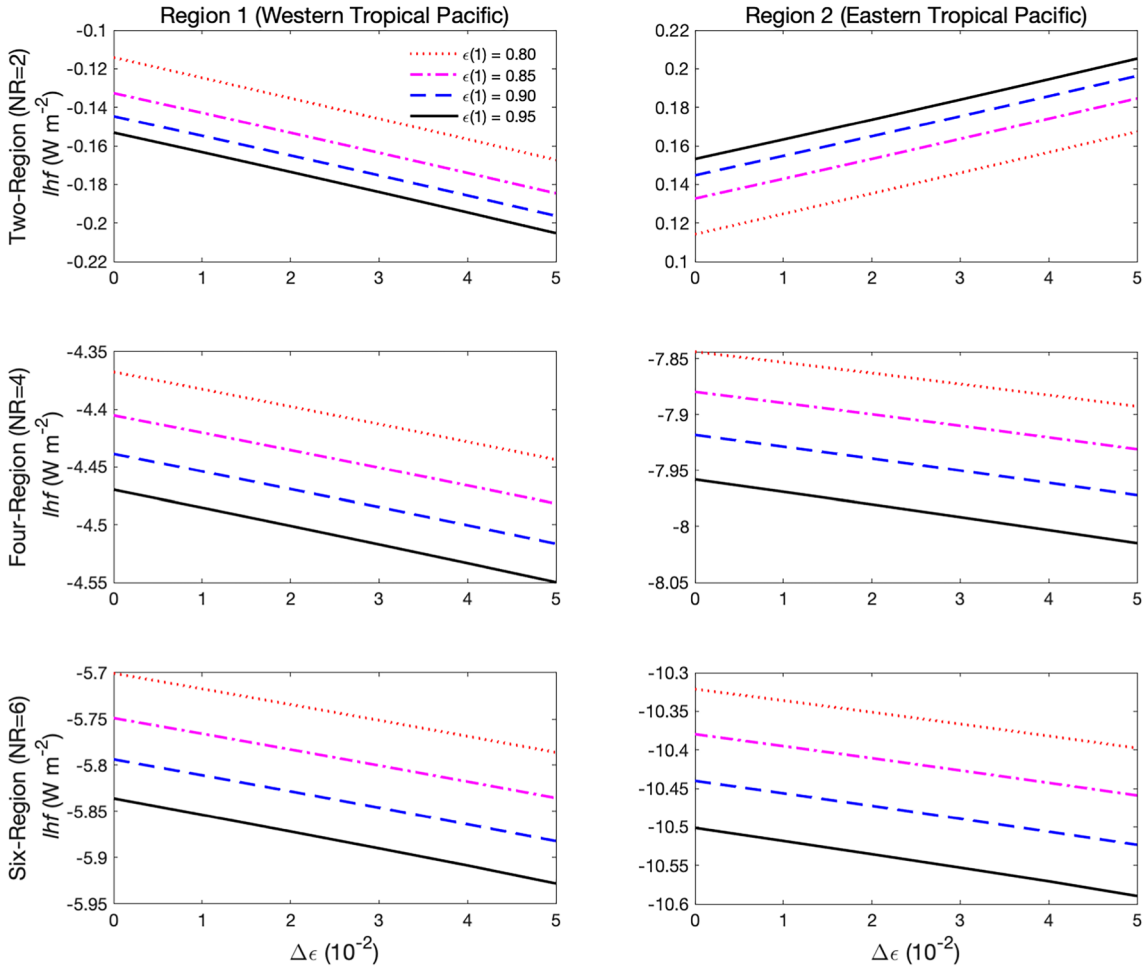

Fig. 5 Same as Fig. 2, except that lateral heat flux convergence is shown

3.3 Sensitivity of Zonal Gradients in Tropical Pacific Climate to Extratropics

Additionally, the zonal gradients of T_{sfc} and P_{sfc} are sensitive to the inclusion of the extratropical regions, with the magnitude of the gradients getting larger (i.e., stronger Walker circulation) as more extratropical regions are included (compare the three columns in Fig. 4). In our model, the strengthening of the Walker circulation is caused by heat loss to the extratropics being greater in the eastern tropical Pacific region than in the western region (Fig. 5). Although the mechanism differs, this sensitivity to the presence of the extratropics is consistent with earlier findings. Liu and Huang (1997) considered the idealized atmosphere–ocean coupled system studied by McWilliams and Gent (1978) and proposed that the zonal temperature contrast in the tropics is limited by the temperature difference between the tropics and the extratropics. The idea is that the westward surface wind generates the zonal SST gradient, and since this surface wind is part of the Hadley circulation whose strength is proportional to the meridional temperature gradient, the zonal SST gradient increases as the meridional temperature gradient increases. Unlike the models that these two earlier studies considered, our model neither includes the dynamics of the Hadley circulation nor the wind-driven ocean circulation, yet it arrives at the same conclusion.

Our result that the strengthening of the Walker circulation is caused by heat loss to the extratropics being greater in the eastern tropical Pacific region is supported by observations. Figure 6 shows poleward heat transport across 30°N and 30°S carried out by waves of zonal wavenumbers $k \geq 4$. This choice is made based on the finding by Baggett and Lee (2015) who showed that heat flux by waves with $k \geq 4$ is downgradient, a behavior expected from a heat engine such as the system of our model. Waves of $k \leq 3$ behave differently, as their heat flux is not downgradient and instead depends on the zonal contrast in convective heating. This Rossby wave dynamics is not included in our model. Figure 6 shows that across 30°N, heat flux is greater in the eastern tropical Pacific. Similar zonal variation is not present in the heat flux across 30°S, however.

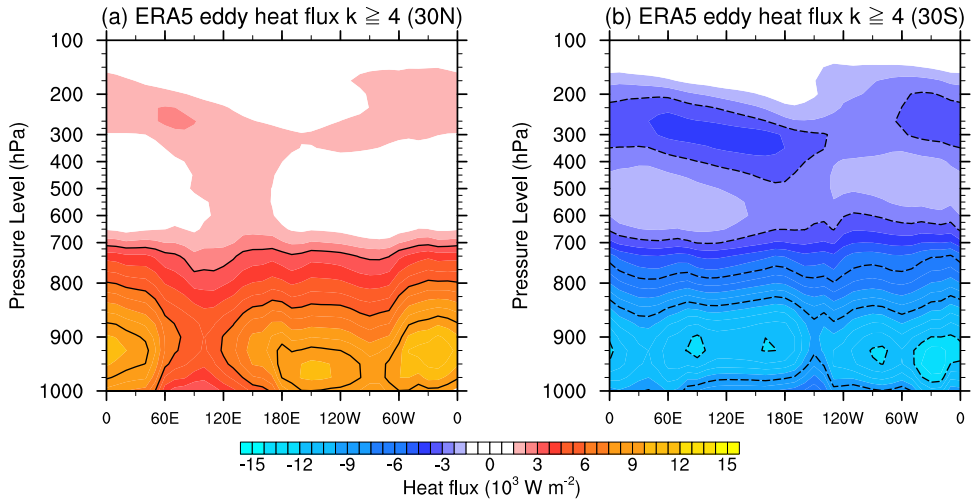

Fig. 6 Annual-mean poleward heat flux carried out by waves with k≥4 across (a) 30°N and (b) 30.°S whose direction is down gradient of the meridional temperature field. The data is from ERA5 reanalysis for the period of 1979–2020. The flux was obtained by first multiplying eddy (deviation from the zonal average) potential temperature and meridional wind at each longitudinal grid point and at each pressure level. The unit is converted to Wm^{-2} by multiplying the specific heat capacity of air at constant pressure and the annual-mean air density, as in Park and Lee 2022). For visualization, a running average across a width of 120-degree longitudes was applied at an interval of 10-degree longitudes. Black contours denote an interval of $3 \times 10^3 Wm^{-2}$

4 Conclusions

In the idealized climate system that we considered, the maxMEP solution shows that a uniform increase in longwave absorptivity results in greater zonal contrasts in surface temperature, surface pressure, and convective heating across the tropical Pacific. This finding raises the possibility that the increased GHG loading in the atmosphere has contributed to the observed strengthening of the Walker circulation and La Niña-like trend. The model input includes climatological shortwave radiation flux at TOA and at surface, hence also the albedo, and the absorptivity of the shortwave. The base-state longwave absorptivity values were tuned to produce realistic surface temperature differences between the six regions. Therefore, the temperature and heat flux solutions of the base states are, to some extent, built in by the input variables. However, the sensitivity of the temperature and heat fluxes to the increases in longwave absorptivity, i.e., GHG forcing, is not built in the model because except for the longwave absorptivity all other input variables are held fixed.

If this maxMEP solution has merit, a natural question is why most of the climate models are predicting El Niño-like trends. A possible answer is that, as pointed out by Johnson (1997), there are aphysical sources of entropy in the climate models which arise from subgrid parameterizations and numerical artifacts including Gibbs oscillations. In such a system with these aphysical entropics, solutions similar to those based on the maxMEP hypothesis may not be realized. Building a climate model with no aphysical sources of entropy to see if the model response to GHG forcing is consistent with our maxMEP solution is beyond the scope of this study.

Our solution also shows that these zonal contrasts across the model's tropical Pacific increase when extratropical regions are added to the climate system. Extratropical impact on tropical zonal contrasts has long been appreciated (McWilliams and Gent 1978; Liu and Huang 1997; Burls and Fedorov 2014). In these studies, the explanations involve ocean dynamics which is not included in our model. Instead, in our model the presence of the extratropical regions strengthens the tropical zonal contrast by importing more heat from the eastern tropical Pacific region than from the western tropical Pacific region. Across 30°N, observed poleward flux by eddies (k≥4 which obeys the flux-gradient relationship) is indeed stronger from the eastern tropical Pacific. Perhaps the effect of the ocean dynamics is implicitly included in our model because the observation-based radiative fluxes and their absorptivities are used as the model input. However, if that were the case, our analysis shows that the stronger heat export from the eastern tropical Pacific is part of the physical picture.

As was stated in the introduction, we view the maxMEP solution as a statistical inference rather than a definite answer. The prediction made by maxMEP is as good as how accurately our idealized climate system captures the essence of the real climate system. The model considered in this study does not, at least explicitly, include numerous processes that probably play a role in determining how the real tropical Pacific responds to GHG warming; ocean dynamics, moisture dynamics, planetary-scale wave

dynamics, stratospheric dynamics, etc. Nevertheless, it is our view that it is useful to know that in the simple climate system under consideration, the maxMEP solution – with its global constraint—predicts that increasing greenhouse gas loading in the atmosphere would result in a more La Niña-like future. This finding underscores the conclusion of the recent review on the subject (Lee et al. 2022) that there is a reasonable chance that the GHG warming has been contributing to the observed trend of the increasing zonal contrasts.

Acknowledgements This study was supported by the National Science Foundation grant AGS-1948667. Conversation with Jerry Harrington inspired the use of maxMEP for this study.

Declarations

Conflict of Interest The authors declare that they have no conflict of interest.

References

Baggett, C., Lee, S.: Arctic Warming Induced by Tropically Forced Tapping of Available Potential Energy and the Role of the Planetary-Scale Waves. J. Atmos. Sci. **72**, 1562–1568 (2015)

Bruers, S.: A discussion on maximum entropy production and information theory. J. Phys. A **40**, 7441–7450 (2007)

Burls, N.J., Fedorov, A.V.: What Controls the Mean East-West Sea Surface Temperature Gradient in the Equatorial Pacific: The Role of Cloud Albedo. J. Clim. **27**, 2757–2778 (2014)

Chou, C., Wu, T.-C., Tan, P.-H.: Changes in gross moist stability in the tropics under global warming. Clim. Dyn. **41**, 2481–2496 (2013)

Clement, A.C., Seager, R., Cane, M.A., Zebiak, S.E.: An Ocean Dynamical Thermostat. J. Clim. **9**, 2190–2196 (1996)

Dewar, R.C.: Information theory explanation of the fluctuation theorem, maximum entropy production and self-organized criticality in non-equilibrium stationary states. J. Phys. a: Math. Gen. **36**, 631 (2003)

Dewar, R.C.: Maximum entropy production and the fluctuation theorem. J. Phys. a: Math. Gen. **38**, L371 (2005)

Dewar, R.C.: Maximum Entropy Production as an Inference Algorithm that Translates Physical Assumptions into Macroscopic Predictions: Don't Shoot the Messenger. Entropy **11**, 931–944 (2009)

Dong, Y., Armour, K.C., Battisti, D.S., Blanchard-Wrigglesworth, E.: Two-way teleconnections between the Southern Ocean and the tropical Pacific via a dynamic feedback. J. Clim. **35**(19), 6267–82 (2022)

Goody, R.: Maximum Entropy Production in Climate Theory. J. Atmos. Sci. **64**, 2735–2739 (2007)

Grinstein, G., Linsker, R.: Comments on a derivation and application of the 'maximum entropy production' principle. J. Phys. A **40**, 9717–9720 (2007)

Hartmann, D. L.: Global Physical Climatology, 2nd ed. Elsevier Science (2016)

Hartmann, D.L.: The Antarctic ozone hole and the pattern effect on climate sensitivity. Proc. Natl. Acad. Sci. **119**, e2207889119 (2022)

Hoskins, B.J., Karoly, D.J.: 1981: The Steady Linear Response of a Spherical Atmosphere to Thermal and Orographic Forcing. J. Atmos. Sci. **38**, 1179–1196 (1981)

Jaynes, E.T.: Information Theory and Statistical Mechanics. Phys. Rev. **106**, 620–630 (1957)

Johnson, D.R.: "General Coldness of Climate Models" and the Second Law: Implications for Modeling the Earth System. J. Clim. **10**, 2826–2846 (1997)

Knutson, T.R., Manabe, S.: Time-Mean Response over the Tropical Pacific to Increased C02 in a Coupled Ocean-Atmosphere Model. J. Clim. **8**, 2181–2199 (1995)

Lee, S., L'Heureux, M., Wittenberg, A.T., Seager, R., O'Gorman, P.A., Johnson, N.C.: On the future zonal contrasts of equatorial Pacific climate: Perspectives from Observations, Simulations, and Theories. npj Clim Atmos Sci **5**, 82 (2022)

Liu, Z., Huang, B.: A coupled theory of tropical climatology: Warm pool, cold tongue, and Walker circulation. J. Clim. **10**, 1662–1679 (1997)

Lorenz, E.N.: Generation of available potential energy and the intensity of the general circulation. In: Pfeffer, R.L. (ed.) Dynamics of Climate, pp. 86–92. Pergamon, Tarrytown, N. Y. (1960)

McWilliams, J.C., Gent, P.R.: A Coupled Air and Sea Model for the Tropical Pacific. J. Atmos. Sci. **35**, 962–989 (1978)

Nelder, J.A., Mead, R.: A simplex method for function minimization. Comput. J. **7**, 308–313 (1965)

Ozawa, H., Ohmura, A., Lorenz, R.D., Pujol, T.: The second law of thermodynamics and the global climate system: A review of the maximum entropy production principle. Rev. Geophys. **41**(4), 1018 (2003)

Paltridge, G.W.: Global dynamics and climate - a system of minimum entropy exchange. Q. J. R. Meteorol. Soc. **101**, 475–484 (1975)

Park, M., Lee, S.: Which Is the More Effective Driver of the Poleward Eddy Heat Flux Variability: Zonal Gradient of Tropical Convective Heating or Equator-to-Pole Temperature Gradient? J. Atmos. Sci. **79**, 1713–1725 (2022)

Pascale, S., Gregory, J.M., Ambaum, M.H.P., Tailleux, R., Lucarini, V.: Vertical and horizontal processes in the global atmosphere and the maximum entropy production conjecture. Earth Syst. Dynam. **3**, 19–32 (2012)

Seager, R., Cane, M., Henderson, N., Lee, D.-E., Abernathey, R., Zhang, H.: Strengthening tropical Pacific zonal sea surface temperature gradient consistent with rising greenhouse gases. Nat. Clim. Chang. **9**, 517–522 (2019)

Seager, R., Henderson, N., Cane, M., M.: Persistent Discrepancies between Observed and Modeled Trends in the Tropical Pacific Ocean. J. Clim. **35**, 4571–4584 (2022)

Shannon, C.E.: A Mathematical Theory of Communication. Bell. System Tech. J. **27**(379), 623 (1948)

Singh, M.S., O'Neill, M.E.: The climate system and the second law of thermodynamics. Rev. Mod. Phys. **94**, 015001 (2022)

Trenberth, K.E., Fasullo, J.T., Kiehl, J.: Earth's Global Energy Budget. Bull. Am. Meteor. Soc. **90**, 311–324 (2009)

Wills, R.C., Levine, X.J., Schneider, T.: Local Energetic Constraints on Walker Circulation Strength. J. Atmos. Sci. **74**, 1907–1922 (2017)

Xie, S.-P., Deser, C., Vecchi, G.A., Ma, J., Teng, H., Wittenberg, A.T.: Global Warming Pattern Formation: Sea Surface Temperature and Rainfall. J. Clim. **23**, 966–986 (2010)